Correlation between microstructure and optical properties of ZnO nanoparticles synthesized by ball milling

P. K. Giri[a)]
Department of Physics and Centre for Nanotechnology, Indian Institute of Technology Guwahati, Guwahati 781039, India

S. Bhattacharyya
Department of Physics, Indian Institute of Technology Guwahati, Guwahati 781039, India

Dilip K. Singh
Center for Nanotechnology, Indian Institute of Technology Guwahati, Guwahati 781039, India

R. Kesavamoorthy, B. K. Panigrahi, and K. G. M. Nair
Materials Science Division, Indira Gandhi Centre for Atomic Research, Kalpakkam 603102, India

Zinc oxide (ZnO) nanoparticles (NPs) in the size range $\sim 7-35$ nm are synthesized by ball-milling technique, and microstructural and optical properties of the NPs are studied using varieties of techniques. Results from ball-milled NPs are compared with those of the commercially available ZnO nanopowder. X-ray diffraction pattern of the milled NPs indicates lattice strain in the NPs. High-resolution transmission electron microscopy analysis reveal severe lattice distortion and reduction in lattice spacing in some of the NPs. Optical absorption spectra of milled NPs show enhanced absorption peaked at 368 nm, which is blueshifted with reference to starting ZnO powder. Room-temperature photoluminescence spectra show five peaks consisting of ultraviolet and visible bands, and relative intensity of these peaks drastically changes with increasing milling time. Raman spectra of milled powders show redshift and broadening of the Raman modes of ZnO, and a new Raman mode evolve in the milled NPs. A correlation between the microstructure and optical properties of ZnO NPs is made on the basis of these results. Our results clearly demonstrate that commercially available ZnO nanopowders do not exhibit nanosize effects due to relatively large size of the ZnO NPs. Implications of these results are discussed. © *2007 American Institute of Physics*. [DOI: 10.1063/1.2804012]

I. INTRODUCTION

Nanostructured ZnO materials have drawn broad attention due to their potential applications in electronics, optics, and photonics.[1–5] In particular, nanosize ZnO finds wide applications in ultraviolet (UV) lasers, solar cells, capacitors, varistors, gas sensors, transparent UV resistance coating, photoprinting, electrophotography, electrochemical and electromechanical nanodevices, sunscreen lotion (cream), cosmetic and medicated creams, etc.[6–9] Some of the future applications include catalysts for organic reactions[10] and delivering drugs to infected areas of body.[11] The optical properties of the ZnO depend closely on the microstructures of the materials, including crystallite size, orientation, and morphology, defects, lattice strain etc. ZnO nanoparticles (NPs) with controlled size and structure are necessary to study their size-dependent properties and explore its applications in the diverse areas of nanotechnology. Therefore, it is necessary to look for simpler approaches for synthesis of ZnO NPs in the ultrasmall size range where quantum confinement effect and surface effects may be prominent and study their structure-dependent properties. While a majority of the studies has focused on the optical properties of ZnO

nanostructures, to date very few studies have been carried out to understand the microstructure of ZnO NPs.

Several physical[2–5,12,13] and chemical techniques[14,15] have been used to synthesize ZnO NPs and thin films. A majority of these techniques is based on bottom-up approach for the growth of ZnO NPs from appropriate precursors or source materials, where the product yield is usually low and impurity content may be high. On the other hand, top-down approaches such as ball milling are relatively less explored for the preparation of ZnO NPs.[16,17] Ball milling is considered as an effective and simple technique to synthesize nanocrystalline particles because of its simplicity, relatively inexpensive equipment, and applicability to essentially all classes of materials. Ball-milling technique has been successfully used to synthesize varieties of semiconducting nanomaterials,[18–21] magnetic nanomaterials,[22] carbon nanotubes,[23] boron nitride nanotubes,[24] etc. Ball milling lowers the melting point, leading to the synthesis of nanomaterials at relatively low temperatures. Homogeneously sized NPs and nanocomposites can be synthesized depending on ball size and milling time. It operates at room temperature, increasing safety and reducing energy consumption, and no gaseous emissions are produced.[25] It has been reported that ball milling not only induces morphological and structural changes in the particles, but also changes its electrical[26] and optical[19] properties. Ball-milling technique has been success-

---

a)Electronic mail: giri@iitg.ernet.in

102, 093515-1

fully used to grow ZnO nanowires,[20] nanobelts, nanorods,[25] etc. from milled powders of ZnO, and it offers a convenient means to manipulate material properties at nanoscale. However, size-dependent properties and the correlation of microstructure and optical properties of ZnO NPs prepared by ball milling have not been studied systematically in the literature.

In this paper, we report on the synthesis of ultrasmall ZnO NPs using ball-milling technique and study the structural, vibrational, and optical properties of these NPs. Structure and morphology of the milled ZnO NPs are studied by x-ray diffraction (XRD), transmission electron microscopy (TEM), atomic force microscopy (AFM), and dynamic light scattering (DLS), while optical properties are studied using UV-visible absorption, photoluminescence, and Raman scattering techniques. Through this study, we attempt to correlate the microstructure, light absorption and emitting properties of the ZnO NPs. Our results are compared with those of the commercially available ZnO nanopowder.

II. EXPERIMENTAL DETAILS

Commercially available pure ZnO powder (Merck, >99%) was used as the starting material. The particle sizes in the starting ZnO powder was >300 nm. The ZnO powder was milled in a mechanical milling machine at 300 rpm for durations of 15 and 25 h in a stainless-steel vial under atmospheric pressure and temperature. Stainless-steel balls of diameter ~6 mm were used in this experiment. The ball to ZnO powder weight ratio was taken as 20:1. Very fine nanopowders with few nanometers were obtained after milling. The structural and the optical properties of the milled nanopowders were studied as a function of milling time, and the results are compared with those of the commercially available ZnO nanopowder (Sigma Aldrich, 99.999%). For subsequent discussion on different samples, we denote the starting ZnO powder as ZnO_0, commercial ZnO nanopowder as ZnO_nano, 15 h milled sample as ZnO_15, and 25 h milled sample as ZnO_25.

In order to study the particles size, stress and the structural changes after milling, x-ray diffraction (XRD) data were obtained with a powder diffractometer (Seifert 3003 T/T). Cu Kα radiation was used with a Ni filter. An AFM (Digital Instruments Nanoscope III) was used to study the morphology of the particles in commercial nanopowder and milled NPs. A 200 KV ultrahigh-resolution TEM (JEOL-2010) was used to study the nanocrystallite size and microstructure the ball-milled NPs. Optical properties of the NPs were studied using UV-visible absorption, photoluminescence (PL), and Raman measurements. Absorption spectra were recorded using a commercial spectrophotometer (Shimadzu 3101 PC). PL spectra were obtained at room temperature using a He-Cd laser (325 nm) as an excitation source and Jobin-Yvon T64000 spectrometer equipped with a cooled charge-coupled detector. Scanning electron microscopy (SEM) (Model LEO 1430VP) was used for studying morphology of particles in ZnO_0 and ZnO_nano samples. Energy-dispersive x-ray (EDX) analysis was performed using the same SEM to estimate the impurity content and chemical composition of different samples. Raman spectra
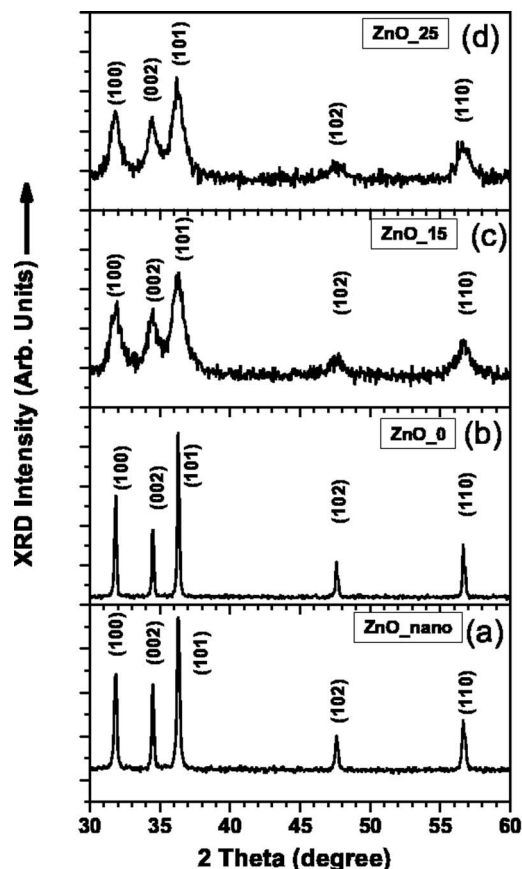

FIG. 1. XRD patterns of (a) commercial ZnO nanopowder; (b) starting ZnO powder; (c) 15 h milled ZnO powder; and (d) 25 h milled ZnO powder.

were recorded in the backscattering geometry using a vertically polarized 488 nm Ar-ion laser beam, a double-grating monochromator, and a cooled photomultiplier tube. All the measurements were carried out at room temperature. Size distribution of the NPs was measured using a commercial particle size analyzer (Horiba LB-550) based on dynamic light scattering (DLS) technique.

III. RESULTS AND DISCUSSION

A. Structure and morphology of ZnO NPs

Figure 1 depicts the XRD pattern obtained for the ZnO_0, ZnO_nano, ZnO_15, and ZnO_25. Structural changes occurring in the ZnO powder could be seen with increasing milling time. All these samples show hexagonal ZnO crystalline structure with varying degree of crystallinity and crystallite size. It may be noted that XRD linewidth of commercial ZnO nanopowder and starting ZnO powders are quite similar, indicating a large average size of the NPs in the commercial nanopowder. With reference to spectrum of ZnO_0 sample, a slight upshift of the XRD peak positions in ZnO_15 and ZnO_25 samples is indicative of compressive strain in milled samples. For (100) plane, we estimate a reduction in interplanar spacing (*d*) of ~0.26% for ZnO_15 sample. ZnO_25 sample did not show any further change in particle size and strain. The broadening of the XRD line profile for the milled NPs, as shown in Fig. 1, can be attributed to the reduction in average particle/crystallite size and

strain induced by the milling process.[16] Average crystallite size and strain in the NPs were calculated from the spectral line shape using Williamson-Hall (WH) plot based on the equation[27]

$$\beta \cos \theta_B = \frac{0.9\lambda}{t} + 4\varepsilon \sin \theta_B, \tag{1}$$

where β, θ_B, λ, t, and ε represent full width at half maximum (FWHM) of the XRD peak, Bragg's angle, wavelength of X-ray ($\lambda = 0.154\,056$ nm), average particle size (diameter), and strain, respectively. Estimations of the average particle size and strain using Eq. (1) assume isotropic strain on the milled NPs, which does not hold true for most semiconductors having directional bonding. We find that in the milled samples, the anisotropic strain causes scatter of data points (nonlinearity) in the WH plot and a proper estimation of the particle size has limited accuracy. Since the strain anisotropy analysis is not straightforward for a hexagonal ZnO structure, we ignore the effect of anisotropy on strain and calculate the average crystallite size and strain from Eq. (1); this procedure is known to yield a higher estimate of particle size. Constructing a WH plot (not shown), we find that average crystallite size and strain are 26 ± 2 nm and 0.84%, respectively, for ZnO_15. Analysis on ZnO_25 sample shows almost identical broadening, indicating that average particle size and strain does not change significantly with additional 10 h milling. This is possibly due to grain growth and corresponding strain relaxation during prolonged milling as a result of dynamic heating during milling. It may be noted that commercially procured ZnO nanopowders do not show any significant broadening in XRD line profile with respect to the starting ZnO powder. Hence, the particle sizes are relatively large in the commercial ZnO nanopowder as compared to those produced by ball milling. XRD results indicated an average particle size of ~240 nm and strain of ~0.08% in ZnO_nano sample.

SEM imaging [see Fig. 2(a)] shows that ZnO_0 has particle sizes in the range 200−400 nm with no regular shape. High-resolution AFM images of ZnO_nano and ZnO_15 are shown in Figs. 2(b) and 2(c), respectively. The ZnO_nano has particle sizes in the range 40–100 nm, whereas ZnO_15 sample exhibits very small particle sizes in the range of 10–35 nm. Although the AFM scanning yields an average particle size of ~20 nm for ZnO_15, spherical NPs as small as ~10 nm are clearly seen in Fig. 3(c). Similar size distribution is found for 25 h milled samples, indicating no significant change in particle size after additional 10 h milling. Note that, since the ball-milled NPs can easily agglomerate to form bigger particles, surface morphology studies do not often reveal the actual particle size. Usually it measures the grain size, rather than the individual particle size. SEM studies show that particles are more agglomerated in ZnO_25 sample than in ZnO_15. In ZnO_15, NP size distribution measured from DLS studies are shown in Fig. 2(d) and it shows relatively higher mean sizes (40–50 nm), due to agglomeration of particles. The inset in Fig. 2(d) shows a low-resolution TEM image of ZnO NPs showing spherical shape with a size of ~20 nm. Since the milling was performed in air ambient using stainless-steel balls, possible change in the
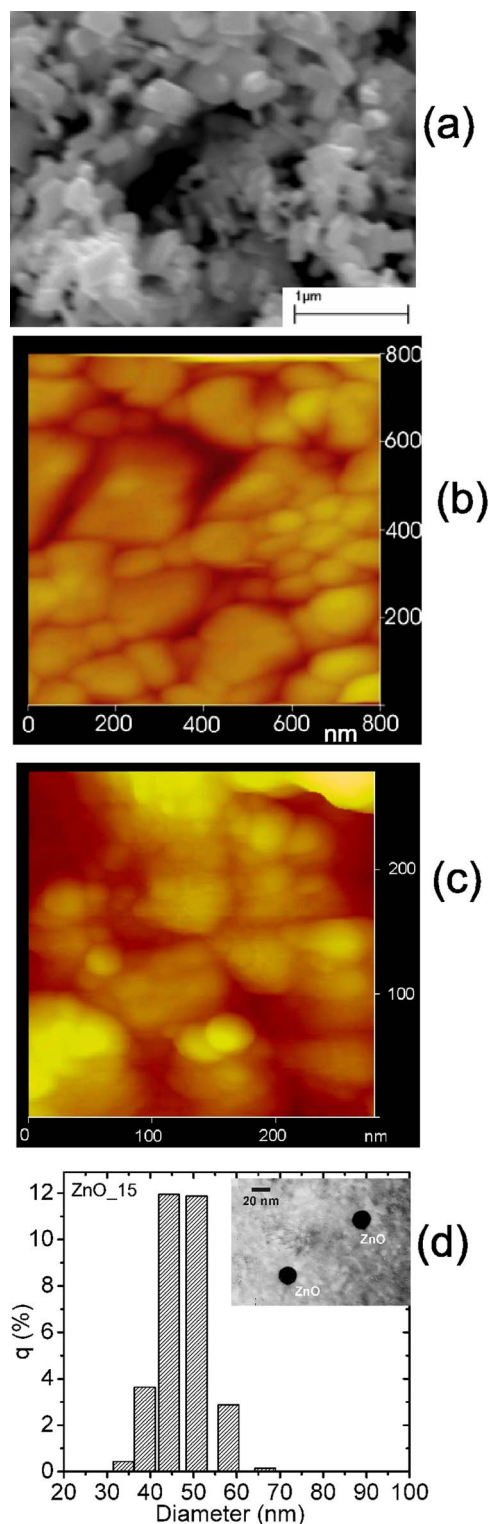

FIG. 2. (Color online) (a) SEM image of starting ZnO powder; (b) AFM image of commercial ZnO nanopowder; (c) AFM image of 15 h milled ZnO powder; and (d) size distribution of NPs measured by DLS technique in ZnO_15. Inset shows a low-resolution TEM image of NPs in ZnO_15 sample.

composition of ZnO and impurity contamination was studied using energy-dispersive x-ray (EDX) analysis. The EDX results are summarized in Table I and, within the limited experimental accuracy, the results show a substantial increase in the oxygen content in ZnO with increasing milling time. It
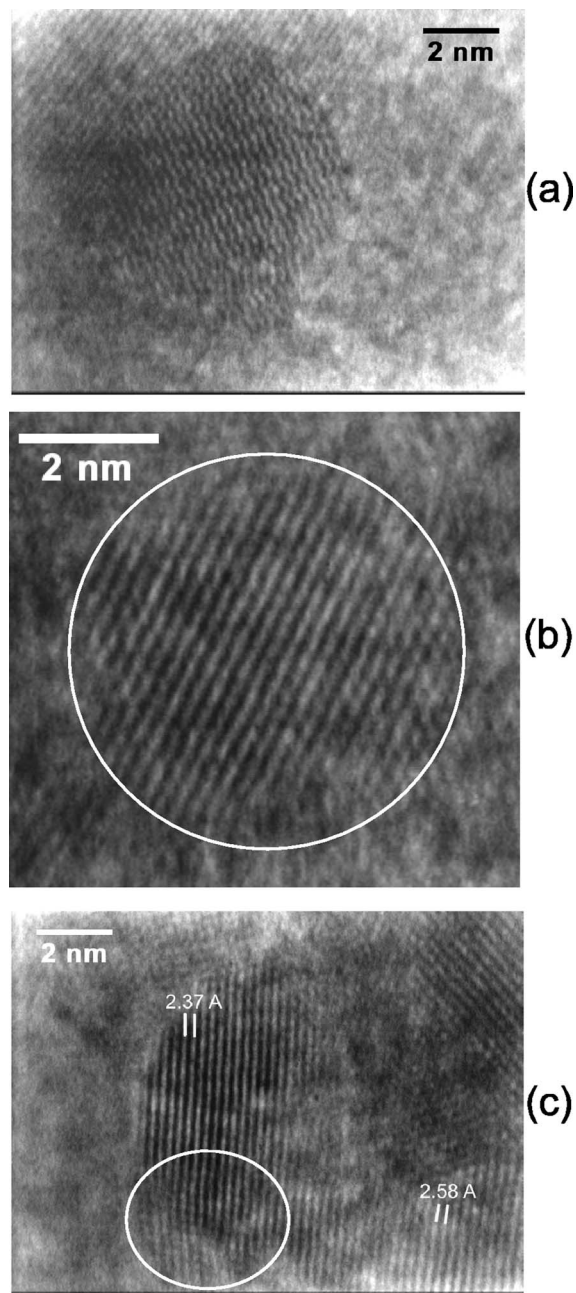
FIG. 3. HRTEM image of ZnO lattice in ZnO_15 sample. (a) A typical crystallite of size ~7 nm; (b) higher resolution image of an ultrasmall crystallite showing no lattice distortion; (c) a small crystallite showing reduced lattice spacing and severe lattice distortion (white oval region). Interplanar spacing *d* for different regions is shown in angstrom units.

TABLE I. Zinc and oxygen content in commercial ZnO nanopowder and ZnO powders before and after milling as measured by EDX.

Sample	Zn (Atomic %)	O (Atomic %)
ZnO_0	47.42	52.58
ZnO_nano	39.60	60.40
ZnO_15	41.03	58.97
ZnO_25	34.88	65.12

shows a set of HRTEM images of the ZnO lattice after 15 h of milling. It is evident from Figs. 3(a) and 3(b) that ZnO NPs as small as 7 nm are formed in ZnO_15 samples having an ordered lattice structure. While no apparent lattice distortion is seen in Fig. 3(b), Fig. 3(c) shows a typical image of lattice distortion in some of the ZnO NPs. Highly distorted region of the lattice is marked with a white oval. Lattice spacing calculated from HRTEM images show that the distorted lattice has a reduced *d* spacing (2.37 Å) as compared to the *d* spacing expected for perfect ZnO crystal. A portion of Fig. 3(c) with a different NP shows a *d* spacing of 2.58 Å that closely matches with the expected *d* spacing for (002) planes. Thus, HRTEM images clearly show a compressive strain in the lattice of some of the NPs. Therefore, ball-milling produces some of the ultrasmall NPs with strain in the lattice. These results are consistent with XRD analyses that also indicated strain and reduction in lattice constant as a result of milling. Note that average strain as calculated from XRD pattern is quite low as compared to the large strain found in some of the NPs as shown in Fig. 3(c). The lattice strain has important bearing on the light emission and phonon modes of the NPs.

B. UV-visible absorption spectroscopy

UV-visible absorption spectra of the ZnO NPs, ultrasonically dispersed in THF (tetrahydrofuran), are shown in Fig. 4. The plotted data are corrected for the solvent contribution. The room-temperature spectra exhibit excitonic absorption feature peaked at ~368 nm for both ZnO_15 and ZnO_25 samples as compared to the 382 nm peak for unmilled ZnO_0. With reference to ZnO_0 and ZnO_nano, the milled NPs show a dramatic increase of absorption intensity and a blueshift of the peak. Note that milled NPs show much higher absorption than that of the commercial ZnO nanopowder. The observed blueshift in ultrasmall NPs is indicative of an increase in band gap. Since the excitonic Bohr diameter is 6.48 nm for ZnO, NPs in the size range 7−8 nm are expected to exhibit quantum confinement effect in the absorption spectra. However, since the average particle sizes are somewhat higher, a weak confinement effect is expected from the milled NPs. Hence, the observed blueshift may be primarily attributed to quantum confinement effect.[28] Based on the effective mass approximation theory by Brus,[28] the observed blueshift yields a NP size of ~5−6 nm. This value is close to the size of ~7 nm as observed by HRTEM. However, since the average size of the NPs in our sample is larger than this size, the observed blueshift cannot not be fully attributed to quantum confinement effect alone. Since a local

may be noted that ZnO_nano also shows high oxygen content similar to that of ZnO_15 sample. High oxygen content in milled samples is due to the milling performed in the air ambient where the ZnO powder reacts with atmospheric oxygen. EDX analyses on milled powders also indicate that a small fraction (0.23–0.42%) of Fe and Cu is introduced as contaminants in ZnO during milling, since iron vials and iron balls were used for milling, and this contamination causes a grayish color of the milled powder as compared to the starting whitish ZnO powder. Such contamination affects the PL characteristics of NPs significantly, as discussed later.

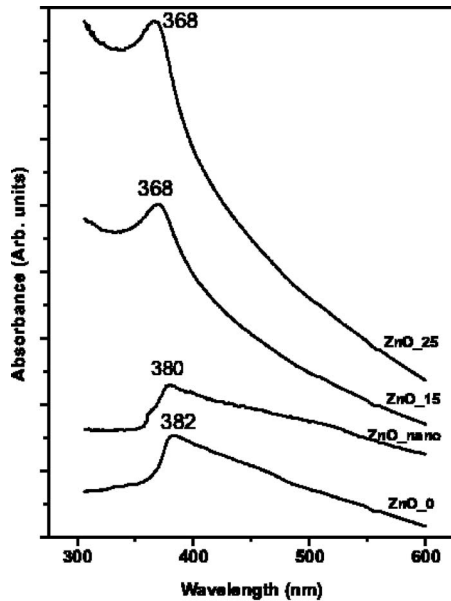The structural modifications of the NPs are further studied by high-resolution TEM (HRTEM) imaging. Figure 3

FIG. 4. UV-visible absorption spectra of starting ZnO powder, commercial ZnO nanopowder, and ball-milled ZnO powders. Peak positions are denoted in nanometer units, which show a clear blueshift in milled NPs.

strain can change the band gap of ZnO NPs, a change in band gap due to the strain may be partly responsible for the observed blueshift. The enhanced absorption in NPs can be due to increased oscillator strength and increased surface area with size reduction. On the other hand, in ZnO_nano sample nanosize effects are not prominent in optical absorption behavior since the particle sizes are much above the confinement region. Hence, commercial ZnO nanopowders with relatively large NPs do not possess the nanosize effect contrary to the expected improvement in the UV absorbance of nanopowder. One the other hand, effect of nanosize on the UV absorbance is very prominent in milled NPs. Since the excitonic absorption is substantially increased in the milled ZnO NPs, these NPs have great potential for use as efficient UV light absorber. This property has recently been exploited in improving the finishing of textile products[29] and ZnO NPs are already being utilized for improved cosmetic products.

C. Photoluminescence spectroscopy

Room-temperature photoluminescence (PL) spectra of all the ZnO samples are shown in Fig. 5. The spectra show emission bands in the UV and visible region with asymmetric line shape. Experimental data are fitted with five constituent peaks (A–E) with Gaussian line shape, and peak positions are extracted from free-parameter fittings as summarized in Table II. Fitted data show that the relative amplitude of these peaks drastically changes with milling time, with a minor shift in the peak positions. The peak A at ~378 nm is due to bound excitonic transitions in ZnO crystallites[30] and the close-by peak B at ~386 nm is likely to be caused by band-to band transition in the band-tail states of ZnO NPs.[31] These band-tail states are primarily caused by disorder/defects at the surface of the NPs. FWHM of peak B gradually increases with milling time as compared to that of peak A, but the intensity of peak A goes down drastically
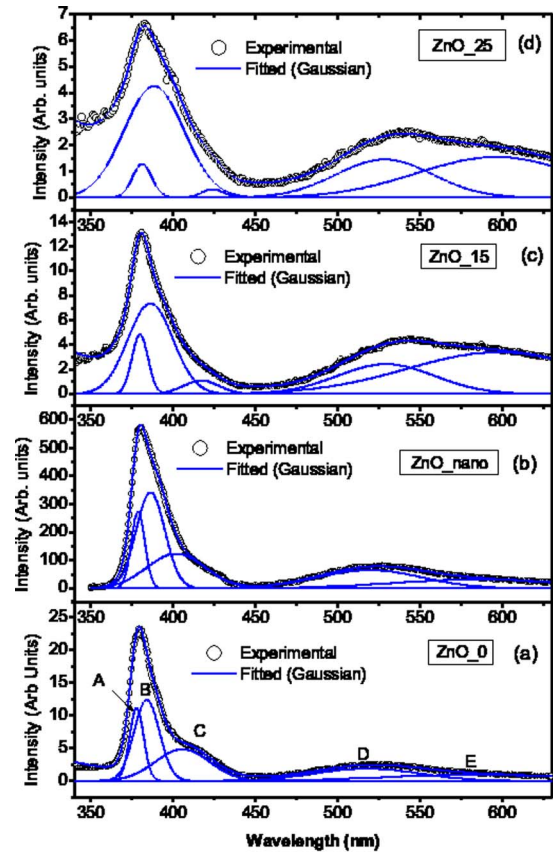

FIG. 5. (Color online) Room-temperature photoluminescence (PL) spectra of the (a) starting ZnO powder; (b) commercial ZnO nanopowder; (c) 15 h milled ZnO powder; and (d) 25 h milled ZnO powder. Altogether, five peaks (marked as A, B, C, D, and E) are fitted with Gaussian line shape (solid line) to the experimental data (symbols). Peak positions are summarized in Table II. Significant changes in relative intensity and linewidth (FWHM) occur as a result of milling.

with milling. From the relative intensity of the peak A and B in different samples as shown in Fig. 5, it is clear that in the milled NPs recombination at band-tail states dominates over the band-edge related transitions. Thus, expected blueshift of UV band (peak A) as a result of quantum size effect is overshadowed by the strong influence of peak B due to surface defects. When the excitons are localized at these defects, exciton energy can be decreased.[32] Therefore, we do not observe any substantial blueshift of peak A with milling time. The peak C at ~405 nm gradually redshifts and FWHM reduces with milling time. Similarly, peak D and peak E redshift with milling, without any significant change in the linewidth. We notice that in the milled NPs the intensity of the all the peaks drastically reduces, except the peak E that grows significantly and is present in commercial nanopowder as well. This peak is primarily due to disorder and strain in the ZnO lattice induced by milling. Lattice strain may change the band structure of the NPs and can introduce nonradiative recombination centers in the band gap. In addition, impurities added during milling may act as nonradiative centers. Iron is a well-known quencher of PL in many fluorophores. As a result, excitonic emission intensity weakens greatly, whereas the intensity of the defect related emissions is relatively less affected. Since the peak E intensity is strong

TABLE II. Summary of the parameters of fitted (Gaussian) peaks to the experimentally observed spectra for different ZnO samples. Peaks *A*, *B*, *C*, *D*, and *E* are marked in PL spectra of Fig. 5. Significant changes in relative intensity of these peaks are observed after milling.

Sample	PL peak positions (nm)				
	A	*B*	*C*	*D*	*E*
ZnO_0	377.8	384.0	405.6	517.7	584.5
ZnO_nano	378.7	386.3	401.0	519.3	585.8
ZnO_15	379.8	386.2	417.1	529.2	597.7
ZnO_25	381.2	388.4	424.1	528.4	596.1
Peak identity	Bound excitons	Band-tail states	V_{Zn}	O_{Zn}	Surface disorder

in milled NPs and also notably present in ZnO_nano, this peak is attributed to surface defects in the NPs. Similarly, gradual increase in intensity and broadening of peak *B* with milling is related to disorder-induced band-tail states in NPs.[31] Peak *C* at ~405 nm has been attributed to transition from oxygen-vacancy related shallow donor level to valence band.[33] This is consistent with our observation, since peak *C* intensity reduces with increasing oxygen content in milled NPs. However, Lin *et al.* have attributed it to zinc vacancy defects.[34] The peak *D* at ~519 nm has been attributed to the singly ionized oxygen vacancy in the ZnO (Ref. 35) or oxygen antisite defect (O_{Zn}).[34] Recently, Borseth *et al.* have attributed the ~2.35 eV (527 nm) emission band to zinc vacancy related defects.[35] Since the oxygen concentration increases in milled samples, concentration of oxygen antisite defects may increase with milling. Thus, we attribute peak *D* to antisite O_{Zn} defect. The broad peak *E* at ~580 nm has not been reported and is unlikely to be related to intrinsic defects. Since the peak is very broad and is prominent in milled samples, it is likely to be related to disorder at the surface of the NPs. It cannot be related to impurities introduced during milling, since this peak is also present in commercial nanopowder. Surface atoms in the as-milled ZnO NPs are expected to experience disorder and strain and, as a result, the peak is very much broadened. Vacancy-type defects have been detected in milled ZnO powders,[17] and extended defects such as dislocations are quite likely to form in milled nanoparticles. Strain field of these defects introduces nonradiative recombination centers; they are likely to be responsible for the weakening of the excitonic emission.

D. Raman spectroscopy

ZnO has a wurtzite structure, which belongs to the space group C_{6v}^4 with two formula units per primitive cell where all atoms occupy C_{3v}. Zone center optical phonons predicted by group theory are $A1+2E2+E1$. Here, $A1$ and $E1$ modes are polar and split into the transverse optical (TO) and longitudinal optical (LO) phonons. In addition, $E2$ mode consists of two modes: $E2_{(high)}$ is associated with the vibration of oxygen atoms and $E2_{(low)}$ is associated with the Zn sublattice.[36] Room-temperature Raman spectra for all the samples are shown in Fig. 6. The spectra show several peaks characteristic of vibrational modes in ZnO. The peak positions and FWHMs are derived by fitting the Lorentzian line shapes to the spectra. A summary of the Raman modes and FWHM of each peak with possible identity are presented in Table III.

Significant changes in peak position and FWHM occur as a result of ball milling. It is clear from Table III that most of the Raman bands show a redshift and an increased FWHM after milling, as compared to the unmilled or commercial nanopowder samples. The broad Raman peak at ~244 cm⁻¹ is attributed to $B_1^{(low)}$ mode. A similar mode has been predicted by Serrano *et al.*[37] and experimentally observed by Agarwal *et al.*[38] A_1 (TO) mode at 380 cm⁻¹ for the starting material disappeared after milling. E_1 (TO) mode observed at ~412 cm⁻¹ for ZnO_0 shifted to lower wave numbers after milling. The modes E_1 (TO) and A_1 (TO) reflect the strength
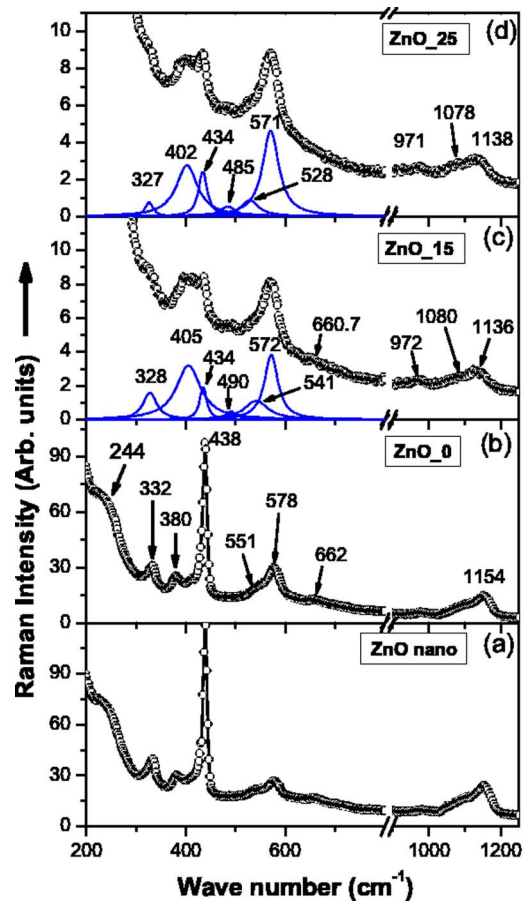

FIG. 6. (Color online) Raman scattering spectra of the (a) commercial ZnO nanopowder; (b) starting ZnO powder; (c) 15 h milled ZnO powder; and (d) 25 h milled ZnO powder. Peak positions are labeled in cm⁻¹ unit. Lorentzian peaks fitted (solid line) to the experimental data (symbols) are shown as solid lines (color) in (c) and (d). Details of all the peaks for different samples are summarized in Table III.

TABLE III. Summary of the Raman modes observed from various samples. Numbers in bracket indicate the FWHM of each peak as determined by fitting Lorentzian line shapes to the observed spectra (Fig. 6). See the text for details on identity of peaks.

Sample	Raman peaks (FWHM in cm^{-1})											
ZnO_0	244.2 (54.0)	332.9 (21.2)	379.9 (27.2)	411.8 (31.9)	438.2 (9.5)	···	551.1 (82.4)	578.9 (26.0)	662 (115.2)	982.9 (49.0)	1102.4 (103.5)	1154.8 (43.0)
ZnO_ nano	241.2 (79.4)	332 (18.6)	386.3 (32.6)	420.6 (26.0)	438.6 (8.6)	···	539.5 (82.3)	578.5 (33.7)	655 (90.2)	981.7 (34.4)	1109 (93.9)	1156.2 (39.8)
ZnO_15	241.2 (79.4)	327.9 (33.5)	ND^a	405.4 (59.5)	434.8 (17.1)	490.4 (28.7)	541.5 (57.2)	571.5 (32.8)	660.7 (32.8)	970.9 (41.0)	1080.4 (74.1)	1136.9 (64.1)
ZnO_25	245.1 (56.2)	326.5 (19.5)	ND^a	402.3 (52.0)	434.2 (20.9)	484.5 (34.6) 528.3 (43.6)	547.6 (5.0)	570.5 (39.8)	ND^a	971.5 (77.8)	1078.4 (82.3)	1138.4 (65.6)
Peak identity	$B_1^{(low)}$	$E_{2H}-E_{2L}$	A_1 (TO)	E_1 (TO)	$E_2^{(high)}$	Surface optical mode	2LA	A_1 (LO)	Multiple-phonon	2TO	A_1, E_2 symmetry	2LO

^{a}ND: below the detection limit.

of the polar lattice bonds. The disappearance of the A_1 (TO) mode and peak shift of the E_1 (TO) mode after milling indicate that there is a change in lattice constants after milling. This is consistent with the HRTEM observations. A_1 (LO) mode observed at 578.9 cm^{-1} has been attributed to oxygen vacancy or zinc interstitial or their complexes.[37] In the milled NPs, oxygen vacancy at the surface of the NPs may be increased as a result of milling; thus, the A_1 (LO) peak intensity does not reduce so much, despite a drastic reduction in intensity of all other peaks. $E_2^{(high)}$ mode at 438 cm^{-1} is most prominent in the starting ZnO material; after milling, intensity of this peak reduces by several fold along with broadening and redshift of the peaks. Generally, the $E_2^{(high)}$ mode represents the band characteristic of wurtzite phase. Lowering in intensity and broadening of 438 cm^{-1} peak indicate a change in band structure of ZnO NPs after milling. This is consistent with the observed change in optical absorption and broadening of the PL emission band. The size reduction and lattice strain reduces the Raman scattering cross section; this effect is dominant for the milled NPs. Peak broadening in milled samples is attributed to size distribution and strain in the NPs. A new low-intensity peak appear at $\sim$490 cm^{-1} after milling; this peak intensity does not increase with increased milling time. Since impurity (Fe and Cu) concentration increases with milling time, impurities are unlikely to be responsible for the new peak. A similar peak has been observed recently by Chassaing *et al.*[39] and was attributed to surface optical phonon modes of small ZnO NPs. Since the numbers of surface atoms are significant in small NPs (a few nanometers), these surface atoms are expected to show up as surface optical phonon mode. Our PL data also support such a view, and we attribute the $\sim$490 cm^{-1} peak to surface optical phonon mode.[39] ZnO_25 sample shows an additional new peak at 528 cm^{-1}, which may originate from disorder-induced allowed Raman transitions.[40] Identities of all other peaks are presented in Table III, in accordance with the reported literature.[37,41]

With reference to ZnO starting powder, redshift of the Raman peaks was about $\sim$4−7 cm^{-1} for all the major peaks after 15 h of milling. There are three possible mechanisms for the phonon peak shifts in Raman spectra of nanostructures. The first one is spatial confinement of phonons within the nanocrystals. The second one is related to the phonon localization by defects. Nanocrystals or quantum dots produced by chemical methods or by physical methods normally have more defects than corresponding bulk crystals. The third one is related to strain-induced shift of phonon modes. Note that we observe a downshift of the Raman modes after milling, contrary to the expected upshift of the Raman modes due to the compressive strain on these NPs. Due to a complex interplay of strain, size distribution, phonon confinement, and defects on the Raman linewidth and peak position, estimation of strain from the Raman spectra is not straightforward. The spatial confinement of optical phonons was studied by Richter *et al.*,[42] who showed that the Raman spectra of nanocrystalline semiconductors are redshifted and broadened due to the relaxation of the q-vector selection rule in the finite-size nanocrystals. On the other hand, Zhang *et al.*[43] showed that ZnO nanoparticle with nearly uniform size do not show any Raman frequency shift with particle size. Optical-phonon confinement in wurtzite nanocrystals leads to slightly different changes in Raman spectra due to the optical anisotropy of wurtzite lattice.[44] Alim *et al.*[45] argued that, although the phonon confinement effect is relatively weak in ZnO nanocrystals, a small redshift of phonon spectra in 20 nm ZnO could be attributed to phonon confinement effect. Since some of the ZnO NPs in our sample are in the weak confinement regime, the measured small redshift may partly be attributed to the size effect. Ashkenov *et al.*[36] attributed small redshift in LO phonon modes in ZnO thin films to vacancy-type defects. Impurity-induced disorder and corresponding relaxation of translational symmetry has also been suggested to cause redshifting of the Raman peak in ZnO.[40] In the present study, the observed redshift for both TO and LO phonon modes is primarily attributed to size effect, and the peak broadening is attributed to strain and size distribution in the NPs.

Despite the presence of ultrasmall NPs in milled ZnO, optical emission characteristics are adversely affected by anisotropic strain and disorder in the NPs. Previous studies have shown that the lattice strain in milled ZnO NPs can be reduced by thermal annealing above 450 °C.[17] However, during annealing the grain size grows and agglomeration of particles takes place. We find that while the optical absorption is enhanced in milled NPs as compared to the commercial nanopowder, the UV emission is weaker in milled NPs primarily due to introduction of nonradiative centers as a result of defects and impurities in the NPs. As ball milling

enables large-scale production of nanoparticles in the quantum size range, this can be a useful choice where large surface/volume ratio is exploited in varieties of applications such as cosmetics, catalysts, drug delivery, etc. Though we have obtained NP sizes ≥ 7 nm, use of smaller ball in the grinding jar may enable production of even smaller particle sizes to exploit further the nanosize properties of ZnO. This method is applicable for large-scale production of other semiconductors NPs as well.

IV. CONCLUSIONS

ZnO NPs in the size range $7-35$ nm were synthesized from commercial ZnO powder using ball milling, and studied for changes in microstructure and optical properties. The XRD pattern indicates strain in the hexagonal lattice of milled ZnO NPs, and HRTEM analysis revealed severe lattice distortion in some of the NPs. EDX analysis showed higher oxygen content in the milled samples as compared to the starting ZnO powder. Observed enhancement of the UV absorption and small blueshift of absorption peak in milled ZnO NPs are attributed to nanosize effects and this is significant for future applications. The band-edge PL emission at room temperature, however, weakens by several fold due to lattice strain and impurities introduced during milling. The new Raman mode at ~ 490 cm^{-1} is attributed to surface phonon modes, and the ~ 528 cm^{-1} peak is caused by disorder-induced relaxation of symmetry properties in the NPs. Redshift and broadening of Raman peaks is attributed to size effect and strain in the NPs. Our results clearly show that commercially available ZnO nanopowders have very large particle sizes compared to the sizes achieved in our study, and the commercial ZnO nanopowder does not show any nanosize effects. Since the particle sizes are relatively large in commercial nanopowder, strain effect is not significant and optical and vibrational properties of commercial nanopowder resemble that of the bulk ZnO powder.

[1] Ü. Özgür, Ya. I. Alivov, C. Liu, A. Teke, M. A. Reshchikov, S. Dogan, V. Avrutin, S.-J. Cho, and H. Morkoç, J. Appl. Phys. **98**, 041301 (2005).
[2] Z. Fan and J. G. Lu, J. Nanosci. Nanotechnol. **5**, 1561 (2005).
[3] Z. L. Wang, J. Phys.: Condens. Matter **16**, R829 (2004).
[4] Y. W. Heo, D. P. Norton, L. C. Tien, Y. Kwon, B. S. Kang, F. Ren, S. J. Pearton, and J. R. LaRoche, Mater. Sci. Eng., R. **47**, 1 (2004).
[5] G.-C. Yi, C. Wang, and W. I. Park, Semicond. Sci. Technol. **20**, S22 (2005).
[6] H. T. Wang, B. S. Kang, F. Ren, L. C. Tien, P. W. Sadik, D. P. Norton, S. J. Pearton, and J. Lin, Appl. Phys. Lett. **86**, 243503 (2005).
[7] J.-J. Wu, G.-R. Chen, H.-H. Yang, C.-H. Ku, and J.-Y. Lai, Appl. Phys. Lett. **90**, 213109 (2007).
[8] S. F. Yu, C. Yuen, S. P. Lau, W. I. Park, and G.-C. Yi, Appl. Phys. Lett. **84**, 3241 (2004).
[9] N. Serpone, D. Dondi, and A. Albini, Inorg. Chim. Acta **360**, 794 (2007).
[10] W. J. Huang, G. C. Fang, and C. C. Wang, Colloids Surf., A **260**, 45 (2005).
[11] C. Dai, B. Wang, and H. Zhao, Colloids Surf., B **41**, 117 (2005).
[12] Z. R. Dai, Z. W. Pan, and Z. L. Wang, Adv. Funct. Mater. **13**, 9 (2003).
[13] B. D. Yao, Y. F. Chan, and N. Wang, Appl. Phys. Lett. **81**, 757 (2002).
[14] C. Wu, X. Qiao, J. Chen, H. Wang, F. Tan, and S. Li, Mater. Lett. **60**, 1828 (2006).
[15] M. Li, H. Bala, X. Lv, X. Ma, F. Sun, L. Tang, and Z. Wang, Mater. Lett. **61**, 690 (2007).
[16] L. C. Damonte, L. A. M. Zelis, B. M. Soucase, and M. A. H. Fenollosa, Powder Technol. **148**, 15 (2004).
[17] S. Dutta, S. Chattopadhyay, D. Jana, A. Banerjee, S. Manik, S. K. Pradhan, M. Sutradhar, and A. Sarkar, J. Appl. Phys. **100**, 114328 (2006).
[18] B. J. Pawlak, T. Gregorkiewicz, C. A. J. Ammerlaan, W. Takkenberg, F. D. Tichelaar, and P. F. A. Alkemade, Phys. Rev. B **64**, 115308 (2001).
[19] Q. Li, C. Liu, Z. Liu, and Q. Gong, Opt. Express **13**, 1833 (2005).
[20] A. M. Glushenkov, H. Z. Zhang, J. Zou, G. Q. Lu, and Y. Chen, Nanotechnology **18**, 175604 (2007); T. Tsuzuki and P. G. McCormick, Scr. Mater. **44**,1731 (2001).
[21] T. Tsuzuki and P. G. McCormick, Nanostruct. Mater. **12**, 75 (1999).
[22] T. D. Shen, R. B. Schwarz, and J. D. Thompson, Phys. Rev. B **72**, 014431 (2005).
[23] Y. Chen, M. J. Conway, and J. D. Fitzgerald, Appl. Phys. A: Mater. Sci. Process. **76**, 633 (2003).
[24] Y. Chen, J. Fitzerald, J.S. Williams and P. Willis, J. Metastable Nanocryst. Mater. **2–6**, 173 (1999).
[25] J. S. Lee, K. Park, M. I. Kang, I. W. Park, S. W. Kim, W. K. Cho, H. S. Han, and S. Kim, J. Cryst. Growth **254**, 423 (2003).
[26] Y. Kuga, M. Shirahige, T. Fujimoto, Y. Ohira, and A. Ueda, Carbon **42**, 293 (2004).
[27] G. K. Williamson and W. H. Hall, Acta Metall. **1**, 22 (1953).
[28] L. E. Brus, J. Chem. Phys. **80**, 4403 (1984).
[29] A. Yadav, V. Prasad, A. A. Kathe, S. Raj, D. Yadav, C. Sundaramoorthy, and Y. Vigneswaran, Bull. Mar. Sci. **29**, 641 (2006).
[30] K. Thonke, Th. Gruber, N. Teofilov, R. Schonfelder, A. Waag, and R. Sauer, Physica B (Amsterdam) **308–310**, 945 (2001).
[31] Q. P. Wang, D. H. Zhang, Z. Y. Xue, and X. T. Hao, Appl. Surf. Sci. **201**, 123 (2002).
[32] F. Demangeot, V. Paillard, P. M. Chassaing, C. Pagès, M. L. Kahn, A. Maisonnat, and B. Chaudret, Appl. Phys. Lett. **88**, 071921 (2006).
[33] H. Wei, Y. Wu, L. Wu, and C. Hu, Mater. Lett. **59**, 271 (2005).
[34] B. Lin, Z. Fu, and Y. Jia, Appl. Phys. Lett. **79**, 943 (2001).
[35] T. M. Børseth, B. G. Svensson, A. Yu. Kuznetsov, P. Klason, Q. X. Zhao, and M. Willander, Appl. Phys. Lett. **89**, 262112 (2006).
[36] N. Ashkenov, B. N. Mbenkum, C. Bundesmann, V. Riede, M. Lorenz, D. Spemann, E. M. Kaidashev, A. Kasic, M. Schubert, M. Grundmann, G. Wagner, H. Neumann, V. Darakchieva, H. Arwin, and B. Monemar, J. Appl. Phys. **93**, 126 (2003).
[37] J. Serrano, A. H. Romero, F. J. Manjon, R. Lauck, M. Cardona, and A. Rubio, Phys. Rev. B **69**, 094306 (2004).
[38] D. C. Agarwal, R. S. Chauhan, A. Kumar, D. Kabiraj, F. Singh, S. A. Khan, D. K. Avasthi, J. C. Pivin, M. Kumar, J. Ghatak, and P. V. Satyam, J. Appl. Phys. **99**, 123105 (2006).
[39] P.-M. Chassaing, F. Demangeot, V. Paillard, A. Zwick, N. Combe, C. Pagès, M. L. Kahn, A. Maisonnat, and B. Chaudret, Appl. Phys. Lett. **91**, 053108 (2007).
[40] R. Cuscó, E. Alarcón-Lladó, J. Ibáñez, L. Artús, J. Jiménez, B. Wang, and M. J. Callahan, Phys. Rev. B **75**, 165202 (2007).
[41] L. Liao, D. H. Liu, J. C. Li, C. Liu, Q. Fu, and M. S. Ye, Appl. Surf. Sci. **240**, 175 (2005).
[42] H. Richter, Z. P. Wang, and L. Ley, Solid State Commun. **39**, 625 (1981).
[43] S. L. Zhang, Y. Zhang, Z. Fu, S. N. Wu, M. Gao, M. Liu, J. Chen, L. Niu, J. Z. Jiang, Y. Ling, Q. Wang, and H. Chen, Appl. Phys. Lett. **89**, 243108 (2006).
[44] V. A. Fonoberov and A. A. Balandin, Phys. Rev. B **70**, 233205 (2004).
[45] K. A. Alim, V. A. Fonoberov, and A. A. Balandin, Appl. Phys. Lett. **86**, 053103 (2005).